Formation of Gold-Silver Hollow Nanostructure via Silver Halide Photographic Processes and Application to Direct Electron Transfer Biosensor Using Fructose Dehydrogenase

Yusuke Okawa*[1], Takenori Shimada[2], and Fumiyuki Shiba[1]

[1] Department of Materials Science, Graduate School of Engineering, Chiba University, 1-33 Yayoi-cho, Inage-ku, Chiba 263-8522, Japan

[2] Department of Image and Materials, Graduate School of Advanced Integration Science, Chiba University, 1-33 Yayoi-cho, Inage-ku, Chiba 263-8522, Japan

Corresponding author: Yusuke Okawa, y_okawa@faculty.chiba-u.jp

Abstract

We first employed conventional silver halide photography techniques for constructing a novel nanostructure for electrochemical application. The photographically generated silver nanofilaments from silver bromide microcrystals through chemical development were treated with a gold complex solution. A novel nanostructure composed of silver and gold with hollow structure was obtained, and immobilized on an electrode. The performance as electrocatalyst for direct electron transfer of fructose oxidase was examined and found to be good for biosensor and biofuel cell applications. The current response was kinetically analyzed with a simple kinetic model. Use of carbon paper for the substrate electrode improved the loading amount of the nanostructure and the electrochemical output.

Keywords

silver halide photography; nanostructure; fructose dehydrogenase; direct electron transfer; biosensor

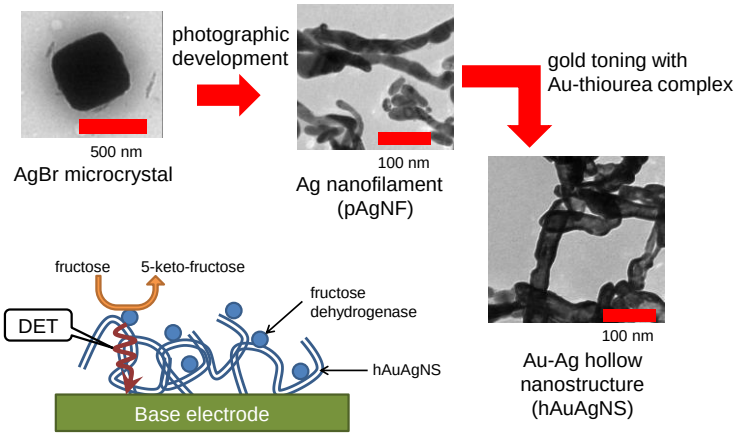

1. INTRODUCTION

Silver halide photography has been, for a long time, a main actor in image recording technology. However, it has gotten off the major leading role because of the recent rapid development of digital electronic imaging technology. Silver halide photography is a fruit of materials technology that has been developed over a century, and fully utilizes the unique characteristics of the element, silver. The accumulation of vast knowledge about the materials technology in silver halide photography should be applied for the other fields.

In conventional silver halide photography, microcrystals of light-sensitive silver halides, i.e., AgCl, AgBr, AgI, and their mixed crystals, are used as photo-recording materials. The light-exposed microcrystals were treated with a solution of reducing agents, a photographic developer, and then the halides are reduced to metallic silver with characteristic filament morphology, "filament silver."[1], [2] The typical width of the filaments is in the order of several tens nm. The deep black tone in silver halide black-and-white photographs is originated from this morphology of the nanoscale filament silver.

Application of nanomaterials, typically nanoparticles and nanowires, to the development of various functional systems has been extensively studied.[3], [4], [5] Metal nanowires featuring high surface area and high electrical conductivity are attractive to design electrochemically functional systems in view of high loading of functional molecules (e.g. enzymes), smooth electron path between the functional molecules and the base electrode[6], and other electrocatalytic [7] and 1-dimensional [8] characteristics. The preparation methods of nanowires and similar morphologies, however, are rather limited relatively to those of nanoparticles. In view of this, silver is one of the widely investigated materials for the formation of such nanostructures.[9], [10], [11]

Formation of filament silver through the photographic development is one of rare examples in view of deeply investigated and well-characterized materials systems, although this characteristic morphology has been less studied for the construction of functional nanosystems.[12] The photographic development could be a potential way to new nanomaterials technology. Combining the established technology in silver halide photography with modern science in, e.g., surface modification, can develop novel functional nanosystems.

In the present study, we apply the photographically prepared silver nanofilaments (pAgNFs) to the construction of electrochemically functional systems for the first time.

Silver as the electrode material features a rather narrow electrochemical window, and relatively easily forms insulating surface derivatives such as oxide and sulfide, being somewhat unattractive for designing electrochemical devices. Problems in the chemical stability of metallic silver have been extensively studied in photographic technology in view of long-term preservation of photographs – especially artistic photographs, historical recordings, and microfilms for archives. Gold deposition of photographic silver is one of the effective means for stabilizing microfilm silver

images.[13] In view of this, we applied the gold deposition technique for improving the electrochemical stability of pAgNF. We found that the deposition process generates a novel hollow nanostructure composed of gold and silver (hAuAgNS).

For the demonstration of a functional design using the silver halide photographic techniques, we further immobilized an enzyme on the photographic nanostructures to fabricate an electrochemical biosensor. Fructose dehydrogenase (FDH, EC 1.1.99.11) is a well-known enzyme which exhibits direct electron transfer (DET) towards various electrode materials, such as carbon,[14], [15], platinum[14], and gold [15], and is extensively studied for the construction of DET-type biosensors [16], [17], [18] and biofuel cells.[19], [20] We introduced FDH to the surface of the photographic nanostructures, and analyzed the response of the novel FDH-based DET biosensors.

2. EXPERIMENTAL

2.1 Materials. As base electrode materials, an indium tin oxide coated glass plate (ITO, 10 Ω/sq, Geomatec) and carbon paper (CP, Toray TGP-H-060) were used. Fructose dehydrogenase (FDH, EC 1.1.99.11, from *Gluconobacter species*) was purchased from Toyobo. A photographic emulsion, composed of mono-disperse pure AgBr cubic microcrystals (edge length of 0.6 μm) dispersed in a aqueous gelatin jelly, was prepared by the controlled double jet technique.[2], [21] Water was purified with deionization and then distillation. The other chemicals are of reagent grade and used as received.

2.2 Synthesis. Under the photographic safe light, the gelatinous photographic emulsion was warmed at 50 °C, spread on a wall of a centrifugal tube, and then cooled with an ice bath for gelation. The emulsion layer set on the wall was then light-exposed with a photographic flashlight, and treated with a photographic developer at 20 °C for 30 min under the safe light. The composition of the developer is based on the conventional D-72 recipe [1], [22] but without potassium chloride (which suppresses photographic fogs in general developing works). The developed emulsion layer was dissolved in a hot water, and the developed silver filaments (pAgNF) were recovered centrifugally, and washed repeatedly by supersonic redispersion in fresh hot water and centrifugal recovery. 2.0 cm^3 of the pAgNF dispersion (1.5×10^{-2} mol-Ag dm^{-3}) was then mixed with 18.0 cm^3 of a gold complex solution including hydrogen tetrachloroaurate(III) and thiourea as the complexation and reducing agent,[13] and kept at 25 °C for 1 h. The recipe of the gold complex solution was based on GP-2,[13], [22] except for the aurate concentration of 1.3 mmol dm^{-3} because of controlling the deposition amount of gold. The treated nanofilaments were recovered and washed by centrifugation.

2.3 Preparation of electrodes. The dispersion was cast on the base electrode (ITO or CP) and naturally dried. The electrode was then immersed with an aqueous solution of 2-mercaptoethanol

(10 mmol dm^{-3}) at 40 °C for 30 min, and thoroughly rinsed with water. A solution of FDH (1 mg cm^{-3}) was dropped on the electrode and allowed for adsorption for 30 min at room temperature.

2.4 Methods. Transmission and scanning electron microscopic observations were conducted with a Hitachi Denshi H-7650 transmission electron microscope and a JEOL JSM-6700 field emission scanning electron microscope, respectively. The energy-dispersion X-ray (EDX) elemental analysis was conducted with the above transmission microscope and the X-ray analyzer module. Electrochemical experiments were conducted with the conventional three-electrode system using a potentiostat (Hokuto Denko Model HB-102 and Toho Giken Model 2000), a home-made Ag/AgCl reference electrode (saturated KCl), and a platinum wire counter electrode at 25 °C. The deposited amount of silver on electrodes was determined by the potentiometric titration with a potassium iodide standard solution after dissolution in a dilute nitric acid and then neutralization.

3. RESULTS AND DISCUSSION

3.1 Characterization of products through photographic processes. Fig. 1(a) illustrates TEM photographs for the developed pAgNF. The thickness of the filaments was roughly from 20 to 50 nm. The pAgNF changes grayish to bluish black within 10 min during the treatment with the gold-deposition solution. Fig. 1(b) shows TEM photograph of the pAgNF after the deposition. The filaments exhibit hollow structure – the transmittance of the electron beam varies clearly between thickly colored walls with the thickness of ca. 10 nm and pale cores. Fig. 1(c) shows SEM image of the gold-deposited sample, illustrating pores on the wall of the developed filaments (see the magnification). Fig. 1(d) gives the result of the EDX elemental analysis for the gold-deposited sample. The nanostructures are composed of silver and gold with the atomic ratio of roughly 1:1. The near uniformity of the elemental composition was confirmed under the present spatial resolution (ca. 100×100 nm^2). However, it is not clear whether deposited gold on the silver wall forms a uniform layer or island-like structure. As well, the peaks of Cu and C in the EDX spectrum are originated from the sample grid.

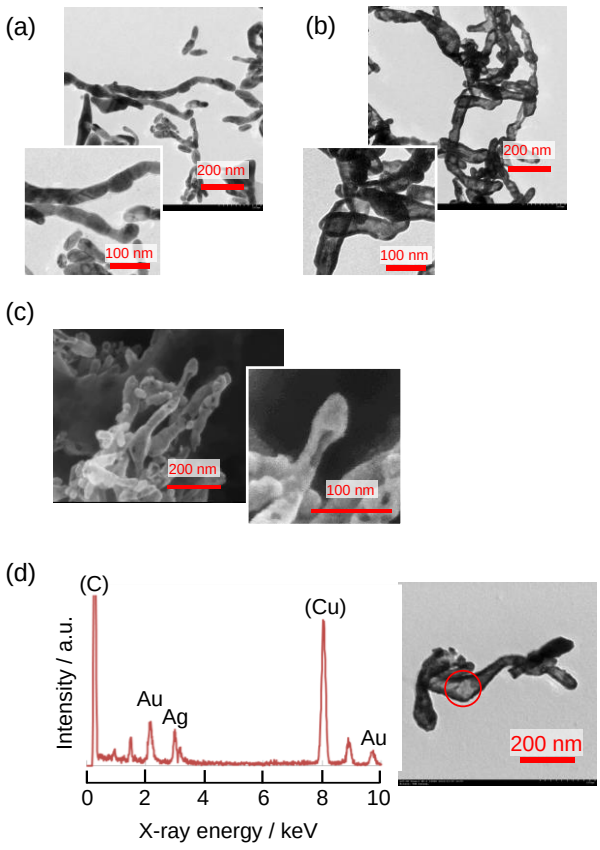

Fig. 1 Transmission electron micrograph of developed silver (pAgNF) (a), gold-deposited pAgNF (hAuAgNS) (b), and scanning electron micrograph of gold-deposited pAgNF (hAuAgNS) (c). A typical TEM-EDX spectrum (d, left) and the corresponding TEM image (d, right) of hAuAgNS (the red circle in the right panel indicates the excitation region for the EDX analysis).

The GP-2 recipe includes hydrogen tetrachloroaurate(III) and thiourea. Thiourea works as the complexation ligand and reducing agent, giving an Au(I)-thiourea complex.[13], [23] Henn and Mack reported in their paper about GP2 treatment of microfilms that the amounts of deposited

gold and dissolved silver were nearly equal, and proposed the following stoichiometry:[13]

$$Au(I) + Ag(0) \rightarrow Au(0) + Ag(I) \qquad (1)$$

In the presence of excess thiourea, Au^+ and Ag^+ both exist as their thiourea-complexes, respectively.

We propose the present model of the formation of the hollow nanostructure as following steps:

1) Metallic gold (Au(0)) is deposited on the filament outer surface through the direct redox reaction between Ag(0) and the Au(I)-complex as shown in Eq. (1).
2) The gold-protected outer surface is roughly completed with some imperfection.
3) Ag(0) at the surface defects galvanically (anodically) dissolves, with simultaneous galvanic (cathodic) deposition of Au(0) from the Au(I)-complex on the gold protective layer. Thiourea also acts as the complexing agent to Ag^+ and assists the dissolution.

   anodic (surface defects): Ag → Ag(I)-thiourea + e^-

   cathodic (deposited gold protective layer): Au(I)-thiourea + e^- → Au(0)

4) Deepening of the dissolution site into the filament interior gives the hollow structure.

The estimated dominant species of the complexes in the present system are $Au(thiourea)_2^+$ and $Ag_2(thiourea)_3^{2+}$ [24], and the redox potentials of the relevant reactions are listed in Table 1. The scheme proposed above is thermodynamically consistent. The detail of the process is currently investigated and will be reported separately.

Table 1. Standard potentials E^o for half reactions relevant to the hAuAgNS formation.

Reaction	E^o / V vs. SHE	Ref.
$formamidine^{2+} + 2e = 2$ thiourea	+0.420	[25]
$Au^{3+} + 2e = Au^+$	+1.401	[26]
$Au(thiourea)^{2+} + e = Au^0 + 2$ thiourea	+0.380	[23]
$Ag_2(thiourea)_3^{2+} + 2e = 2\ Ag_0 + 3$ thiourea	+0.04	[27]*

*The potential was calculated from thermodynamic data given in the literature.

The GP-2 recipe was developed for the protection of microfilms widely used in libraries and archives for the long-term preservation.[13] However, we could not find any papers/reports about the microscopic morphology change of the developed silver. We found that the novel hollow nanostructure is formed through the rather classical method in photographic chemistry. This hollow nanostructure is hereafter referred as hAuAgNS.

3.2 Electrochemistry of nanostructure-carrying electrodes. An aliquot of the aqueous dispersion of pAgNF or hAuAgNS was cast on the ITO electrode (50 μL cm^{-2}) and then naturally dried. The deposited nanostructure layers did not peel off from the base electrode against

immersing the electrode in aqueous media, showing their mechanical stability for electrochemical examination. The pAgNF-carrying electrode (pAgNF/ITO electrode, loaded Ag = 7×10^{-7} mol cm^{-2}) showed electrochemical response in an aqueous KNO_3 solution similar to a silver bulk electrode. However, the reproducibility of the current magnitude was poor, and all the electrodes stored in air for several days after the preparation exhibited no electrochemical response. This is caused by the aerial oxidation (and/or related passivation reactions such as sulfidation) of the pAgNF surface; the oxidized surface works as an insulation layer to the base electrode. On the other hand, the hAuAgNS-carrying electrode (hAuAgNS/ITO electrode, loaded Ag = 5×10^{-7} mol cm^{-2}) showed relatively reproducible current responses, even when stored in air for several days. Gold deposition on pAgNF dramatically improved the stability of the nanostructure surface. It is noteworthy that the redox current responses were quite similar to the freshly prepared pAgNF/ITO electrode, exhibiting that the dominant redox site of the hAuAgNS is silver.

3.3 Application to construction of an FDH-based direct electron transfer enzyme electrode. Fructose dehydrogenase (FDH, EC 1.1.99.11, from *Gluconobacter species*) is a well-known enzyme catalyzing the following reaction:

D-fructose + oxidant → 5-keto-D-fructose + reduced oxidant (2)

The enzyme utilizes various oxidants, such as hexacyanoferrate(III) and 2,4-dichloroindophenol,[28] and has been applied to the construction of bioanalytical systems [29], [30], [31], [32] with such soluble mediators.

The enzyme is also well-known to exhibit direct electron transfer (DET) to various electrodes without soluble mediators, and is extensively applied to constructing biosensors and biofuel cells. The orientation (adsorbed state) of FDH on the electrode substrate is essential for the DET.[33] For gold electrodes, the introduction of 2-mercaptoethanol (ME) as the sublayer is dramatically effective for enhancing the DET.[34] This effectiveness is also reported for the Au nanoparticle (AuNP) system.[35]

We thus introduced FDH and ME to hAuAgNS and studied the DET. Thiols strongly adsorb surfaces of gold, silver, and copper, and are useful for not only controlling surface properties but also protecting the surface with insufficient chemical stability, and are expected to be effective for protection of silver-based nanostructures. We treated the hAuAgNS/ITO electrodes with 10 mmol dm^{-3} aqueous solution of ME at 40 °C for 10 min to introduce ME to the nanostructure surface (ME/hAuAgNS/ITO electrode). FDH was immobilized by adsorption through treating the ME/hAuAgNS/ITO electrode with a 1 mg cm^{-3} FDH aqueous solution for 30 min at room temperature (FDH/ME/hAuAgNS/ITO electrode).

Fig. 2 shows cyclic voltammograms of the FDH/ME/hAuAgNS/ITO electrode in a pH 6.4 phosphate buffer in the absence and presence of 0.2 mol dm^{-3} D-fructose. The start potential was –

0.20 V, and the voltammograms were recorded at successively expanding the scanning potential ranges towards positive direction. In the absence of fructose (left panel), almost negligible current response was observed below +0.60 V. This reflects the passivation (or stabilization) of silver redox by the adsorbed ME. Application of further anodic potential causes desorption of ME and the successive oxidation of the nanostructure (top curve in the left). In contrast, in the presence of fructose (right panel), the oxidation current was observed from ca. –0.1 V. The scans to +0.40 V exhibited monotonic current increase with the applied potential and gave almost identical traces for the forward and reverse scans. The current is due to the DET oxidation of D-fructose. When the scan range was expanded to +0.60 V, the reverse scan was different from the forward one, and the second scan gave the negligible response (not shown in the Figure), exhibiting the serious fouling of the electrode. This fouling probably caused by the oxidative degradation of the hAuAgNS surface and/or desorption of FDH.

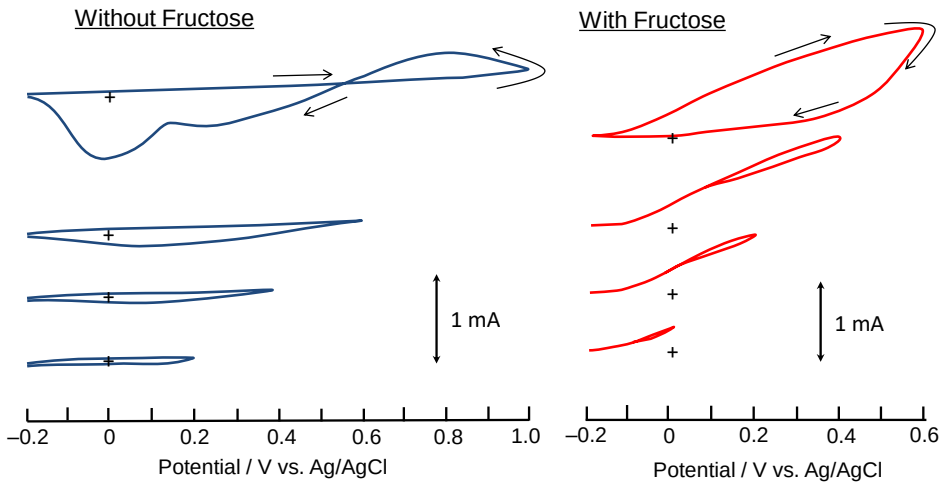

Fig. 2 Cyclic voltammograms for FDH-hAuAgNS electrode in the pH 6.5 phosphate buffer in the absence (left, blue lines) and presence (right, red lines) of 0.2 mol dm^{-3} fructose at successively increasing scanning potential ranges under stirring. Scan rate, 50 mV s^{-1}; start potential, –0.2 V. Cross at each curve indicates the corresponding potential-current origin.

The voltammograms of the fructose DET oxidation (Fig. 2, right panel) do not show the plateau under the sufficient potential application. This suggests that the random orientation of the adsorbed FDH and the dispersion of the DET length (i.e. ET rate) between the redox center of FDH and the hAuAgNS.[36], [37] Controlling the adsorbed/orientation state of the enzyme might improve the working efficiency of the enzyme, and thus the sensor sensitivity. The modification of the nanostructure surface using modifiers other than ME and/or the controlling the preparative conditions of the nanostructure itself could be the future strategy.

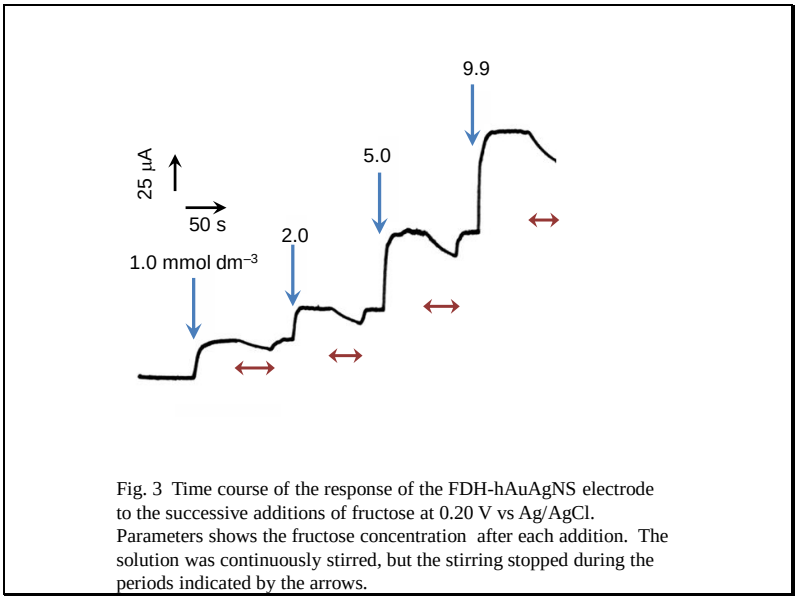

Fig. 3 Time course of the response of the FDH-hAuAgNS electrode to the successive additions of fructose at 0.20 V vs Ag/AgCl. Parameters shows the fructose concentration after each addition. The solution was continuously stirred, but the stirring stopped during the periods indicated by the arrows.

Fig. 3 shows the time course of the current response of the FDH/ME/hAuAgNS/ITO electrode to successive additions of D-fructose standard solution at the constant potential operation. The electrode potential was kept at +0.20 V, and the solution was continuously stirred (ca. 3 rps). After each addition, increase in the oxidation current was observed. The current showed the steady state within 10 ~ 20 s after each addition. The response time is dominantly governed by the mixing and equalization of the solution. When the stirring stopped (indicated by arrows), the current decreased, and the re-starting the stirring recovered the current. This observation indicates the fast surface reaction and the supply of the substrate to the electrode surface is one of the rate limiting steps.

For the purpose of comparison, similar measurements were conducted for the following electrodes.

1) FDH/ME/AuNP/ITO electrode. An ITO electrode carrying gold nanoparticle (AuNP) [38] monoparticular layer was treated successively with ME and FDH with the similar procedure to the hAuAgNS/ITO electrode.
2) FDH/ME/pAgNF/ITO electrode. ME (10 mmol dm^{-3}) was added to the freshly prepared pAgNF dispersion, and the modified pAgNF recovered and washed with centrifugation was immobilized on the ITO electrode. The electrode was finally treated with an FDH solution for absorption and immobilization.

Fig. 4 summarizes the current response of the above three FDH-carrying electrodes as the calibration graph. All the electrodes gave the DET oxidation current but the magnitudes remarkably differ. The introduced amount of pAgNF was estimated to be 7×10^{-7} mol-Ag cm^{-2} and was compatible with the amount of hAuAgNS of 5×10^{-7} mol-Ag cm^{-2}. The remarkable difference in the output currents between hAuAgNS and pAgNF is seen to be caused by the DET efficiency and/or the actively immobilized amount of FDH. Although AuNP is known to be a

favorable DET medium for FDH, the hAuAgNS electrode surpassed the AuNP electrode. This is probably caused by the higher effective surface area from the 3-D structure of the hAuAgNS, giving higher immobilized amount of FDH, and/or DET efficiency on the nanostructures.

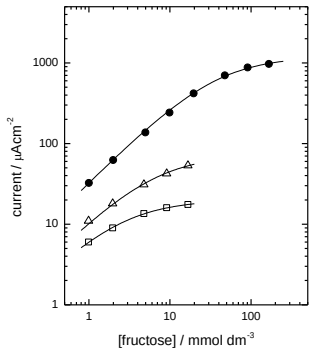

Fig. 4 Calibration graphs for modified electrodes for fructose. ●, hAuAgNS; △, AuNP; □, pAgNF. Working potential, +0.5 V vs Ag/AgCl.

3.4 Kinetic analysis of FDH systems. DET efficiency of the immobilized FDH was evaluated as follows. Although the reaction mechanism of FDH is rather complicated,[39] we employed the following simplified kinetic model:

$$\text{D-fructose} + \text{FDH}_{ox} \xrightarrow{k_c} \text{I} + \text{5-keto-D-fructose} \quad (3)$$

$$\text{I} \xrightarrow{k_e} \text{FDH}_{ox} \quad (4)$$

In this model, oxidized form of FDH (FDH_{ox}) is considered to react to the enzyme substrate, D-fructose, with the apparent rate constant k_c to form the imaginary intermediate (reduced) form of FDH (denoted as I) and the product, 5-keto-D-fructose. The intermediate I is then electrochemically oxidized to FDH_{ox} with the apparent rate constant k_e. In mediator systems, FDH reduced by D-fructose is oxidized by the oxidant through several steps. In DET systems, this process undergoes electrochemically, and the above kinetic model approximates the reaction with an apparent overall rate constant, k_e. The output current density of the electrode is given as

$$i = 2Fk_e[\text{I}]_s \quad (5)$$

where $[I]_s$ is the surface concentration of I. Under the steady state current conditions, the steady state approximation to $[I]_s$, $d[I]_s/dt = 0$, stands, and the solution of the rate equations gives the following equation for the catalytic current density i, when the surface reaction is the rate-determining step of the overall reaction.

$$i = \frac{2F\Gamma_{\mathrm{FDH}}k_{\mathrm{e}}}{1+\frac{k_{\mathrm{e}}/k_{\mathrm{c}}}{[\mathrm{fructose}]}} \qquad (6)$$

where $\Gamma_{FDH} = [FDH_{ox}]_s + [I]_s$ is the total surface concentration of FDH, and F is the Faraday constant. This equation is formally equivalent with the so-called Michaelis-Menten type equation:

$$V = \frac{V_{max}[\mathrm{S}]}{[\mathrm{S}]+K_{\mathrm{m}}} = \frac{V_{max}}{1+\frac{K_{\mathrm{m}}}{[\mathrm{S}]}} \qquad (7)$$

where V is the reaction rate, [S] the substrate concentration, V_{max} the maximum reaction rate, and K_m the Michaelis constant characterizing the enzymatic reaction of interest.

The comparison of Equations (6) and (7) suggests that the apparent K_m value obtained from the analysis of the current-substrate concentration relationship reflects the ratio of the apparent rate constants, k_e/k_c. k_c corresponds to the intermolecular reaction(s) during the substrate and the intermediate state(s) of the enzyme, and is expected to be insensitive (or at least less sensitive) to the nanostructures themselves. This means that the apparent K_m value obtained from the electrochemical responses is a good measure of DET between the enzyme and the nanostructure, and that the higher the apparent K_m value is, the more effective the DET. Note that the apparent K_m value does not depend on the enzyme density.

The solid lines in Fig. 4 are the best fit curves according to Eq. (6), and the experimental data for each electrode well obeyed the Equation. The calculated values of the apparent K_m are 36 mmol dm^{-3} for the FDH/ME/hAuAgNS/ITO electrode, 6.1 mmol dm^{-3} for the FDH/ME/AuNP/ITO electrode, and 2.3 mmol dm^{-3} for the FDH/ME/pAgNF/ITO electrode, exhibiting the highest DET efficiency of the hAuAgNS system. The current of the present system includes the effect from the mass transfer (substrate supply) to the electrode as shown in Fig. 3. Increasing the stirring rate from the present condition, however, enhanced the current in little extent (but the stirring noise in considerable extent for regular experiments), and little affected the apparent K_m value calculated. The current in Fig. 4 is not completely limited by the surface reaction, but the estimation of the apparent K_m value seems thus reasonable. Increase in the loaded amount of hAuAgNS in Section 3.5 (see below) gave the similar value of the apparent K_m, also supporting this conclusion.

FDH carrying DET-type electrodes have been extensively studied and most of them show Michaelis-Menten-type response, and the apparent K_m values for many systems have been reported; for example, 8 mmol dm^{-3} for a carbon paste electrode [14], 9 ~ 10 mmol dm^{-3} for a Ketjen Black system [40], 11 mmol dm^{-3} [39] and 2.3 mmol dm^{-3} [41] for MWCNT systems, 6 mmol dm^{-3} for a polypyrrole-incorporated system [42], and 19 mmol dm^{-3} for a polyaniline-incorporated system.[43]

Although the present results of 6.1 mmol dm^{-3} for AuNP and 2.3 mmol dm^{-3} for pAgNF are comparable to the above reported values, the value of 36 mmol dm^{-3} for hAuAgNS is noteworthily high, strongly evidencing the high DET efficiency on the hAuAgNS.

Although we did not directly determine the immobilized amount of FDH for each electrode, the very large output current for the hAuAgNS system is seen to be due to the larger effective Γ_E than the AuNP and pAgNF systems. Although there are few reports for the DET between FDH and Ag nanostructures, Murata *et al.* [44] reported the DET on an ME-modified silver electrode. We concluded that FDH adsorbed on our ME-modified pAgNF brought about the DET but the absolute amount of effectively working FDH and the efficiency itself were lower than the hAuAgNS system.

In comparison with the AuNP electrode, the hAuAgNS on the electrode features higher effective surface area (with smooth electrical path to the base electrode) resulting in the higher enzyme loading and the higher output current. There probably are nano-scale gold regions on the hAuAgNS surface working as active sites for FDH adsorption and the DET. The nanoscopic characterization of deposited state of gold is ongoing issue for further investigation.

3.5 Use of carbon paper as the base electrode material for the enzyme electrodes. The above experiments were conducted with employing an ITO electrode as the base electrode. However, when the loading amount of the nanostructure increased, the deposited layer tended to peel off. The limitation of the loading amount results in the limitation of the output current. In order to solve this limitation, we tested a carbon paper (CP) with appropriate surface roughness as the basee electrode. For the CP employed in the present work, we successfully and stably increased the loading amount of hAuAgNS by a factor of up to 4.

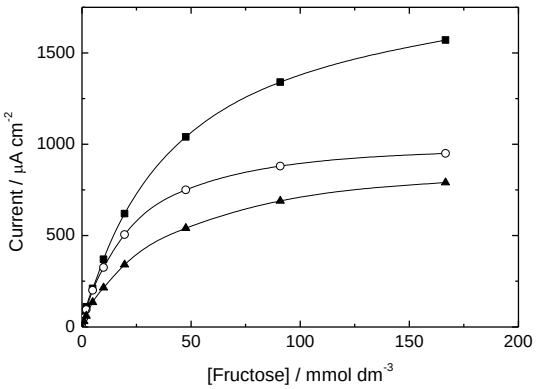

Fig. 5 Calibration graph for FDH/hAuAgNS electrodes. Base electrode, carbon paper (■, ▲), ITO (○). Loaded amount, 5×10^{-7} mol-Ag cm^{-2} (○, ▲), 2×10^{-6} mol-Ag cm^{-2}.

Fig. 5 shows the calibration graph for CP-based electrodes, with comparison of the above ITO-based electrode. When the loading amounts of hAuAgNS are comparable, no remarkable difference was observed for the output currents. However, when the loading amount of hAuAgNS increased by a factor of 4, the current output increased, but by a factor of ca. 2. This is probably caused by the supply (by diffusion) of the enzyme substrate to the interior of the nanostructure layer with a certain thickness. Since the most of the enzyme substrate may completely react with the enzyme in the shallow region of the nanostructure layer, and the deep region of the layer cannot contribute to the output current. The control of the aggregation structure of the nanostructure layer may be of importance to enhancing the overall efficiency and sensitivity of the electrode.

The apparent K_m value for the higher-loading electrode was 37 mmol dm^{-3}, that is comparable with the ITO-based electrode. The DET efficiency is not sensitive to the substrate electrode, and is essentially characteristic to the nanostructure.

4. CONCLUSIONS

We first employed conventional silver halide photography techniques for constructing a novel nanostructure for electrochemical application. A novel hollow nanostructure composed of gold and silver was developed and showed good performance on electrocatalyst for the direct electron transfer of fructose dehydrogenase.

ACKNOWLEDGMENTS

This work was financially supported in part by JSPS KAKENHI Grant-in-Aid for Scientific Research (C) Grant Number G17K05828 and Yutaka Kojima Research Fund of the Society of Photography and Imaging of Japan (2017).

REFERENCES

[1] B.H. Carroll, G.C. Higgins, T.H. James, Introduction to Photographic Theory –The Silver Halide Process–, Wiley, New York, 1980.

[2] T. Tani, Photographic Sensitivity, Oxford University Press, New York, 1995.

[3] X. Luo, A. Morrin, A.J. Killard, M.R. Smyth, Application of nanoparticles in electrochemical sensors and biosensors, Electroanalysis. 18 (2006) 319–326. doi:10.1002/elan.200503415.

[4] A. Walcarius, S.D. Minteer, J. Wang, Y. Lin, A. Merkoçi, Nanomaterials for bio-functionalized electrodes: recent trends, J. Mater. Chem. B. 1 (2013) 4878. doi:10.1039/c3tb20881h.

[5] J. Wang, Nanomaterial-based electrochemical biosensors, Analyst. 130 (2005) 421. doi:10.1039/b414248a.

[6] M.-J. Song, S.W. Hwang, D. Whang, Amperometric hydrogen peroxide biosensor based on a modified gold electrode with silver nanowires, J. Appl. Electrochem. 40 (2010) 2099–2105. doi:10.1007/s10800-010-0191-x.

[7] X. Gao, L. Jin, Q. Wu, Z. Chen, X. Lin, A nonenzymatic hydrogen peroxide sensor based on silver nanowires and chitosan film, Electroanalysis. 24 (2012) 1771–1777. doi:10.1002/elan.201200109.

[8] A.K. Wanekaya, W. Chen, N.V. Myung, A. Mulchandani, Nanowire-Based Electrochemical Biosensors, Electroanalysis. 18 (2006) 533–550. doi:10.1002/elan.200503449.

[9] B. Wiley, Y. Sun, Y. Xia, Synthesis of Silver Nanostructures with Controlled Shapes and Properties, Acc. Chem. Res. 40 (2007) 1067–1076. doi:10.1021/ar7000974.

[10] X. Qin, H. Wang, Z. Miao, X. Wang, Y. Fang, Q. Chen, et al., Synthesis of silver nanowires and their applications in the electrochemical detection of halide., Talanta. 84 (2011) 673–8. doi:10.1016/j.talanta.2011.01.064.

[11] P. Zhang, I. Wyman, J. Hu, S. Lin, Z. Zhong, Y. Tu, et al., Silver nanowires: Synthesis technologies, growth mechanism and multifunctional applications, Mater. Sci. Eng. B. 223 (2017) 1–23. doi:10.1016/J.MSEB.2017.05.002.

[12] T. Tani, Nanoparticles and nanotechnology in silver halide imaging, J. Dispers. Sci. Technol. 25 (2004) 375–388. doi:10.1081/DIS-200025734.

[13] R.W. Henn, B.D. Mack, Gold Protective Treatment for Microfilm, Photogr. Sci. Eng. 9 (1965) 378–384.

[14] T. Ikeda, F. Matsushita, M. Senda, Amperometric fructose sensor based on direct bioelectrocatalysis, Biosens. Bioelectron. 6 (1991) 299–304. doi:10.1016/0956-5663(91)85015-O.

[15] G.F. Khan, H. Shinohara, Y. Ikariyama, M. Aizawa, Electrochemical behaviour of monolayer quinoprotein adsorbed on the electrode surface, J. Electroanal. Chem. Interfacial Electrochem. 315 (1991) 263–273. doi:10.1016/0022-0728(91)80075-2.

[16] L. Gorton, A. Lindgren, T. Larsson, F.D. Munteanu, T. Ruzgas, I. Gazaryan, Direct electron transfer between heme-containing enzymes and electrodes as basis for third generation biosensors, Anal. Chim. Acta. 400 (1999) 91–108. doi:10.1016/S0003-2670(99)00610-8.

[17] R.S. Freire, C.A. Pessoa, L.D. Mello, L.T. Kubota, Direct Electron Transfer: An Approach for Electrochemical Biosensors with Higher Selectivity and Sensitivity, J. Brazilian Chem. Soc. 14 (2003) 230–243.

[18] Y. Wu, S. Hu, Biosensors based on direct electron transfer in redox proteins, Microchim. Acta. 159 (2007) 1–17. doi:10.1007/s00604-007-0749-4.

[19] R.A. Bullen, T.C. Arnot, J.B. Lakeman, F.C. Walsh, Biofuel cells and their development., Biosens. Bioelectron. 21 (2006) 2015–45. doi:10.1016/j.bios.2006.01.030.

[20] J.A. Cracknell, K.A. Vincent, F.A. Armstrong, Enzymes as working or inspirational electrocatalysts for fuel cells and electrolysis., Chem. Rev. 108 (2008) 2439–61. doi:10.1021/cr0680639.

[21] F. Shiba, Y. Okawa, Relationship between Supersaturation Ratio and Supply Rate of Solute in the Growth Process of Monodisperse Colloidal Particles and Application to AgBr Systems, J. Phys. Chem. B. 109 (2005) 21664–21668. doi:10.1021/jp053742t.

[22] S. Anchell, The Dark Room Cookbook, 4th ed., Routledge, Oxon, 2016.

[23] V.P. Kazakov, A.I. Lapshin, B.I. Peshchevitskii, Redox potential of the gold(I) thiourea complex, Russ. J. Inorg. Chem. 9 (1964) 708–709.

[24] J.-Y. Li, X.-L. Xu, W.-Q. Liu, Thiourea leaching gold and silver from the printed circuit boards of waste mobile phones, Waste Manag. 32 (2012) 1209–1212. doi:10.1016/j.wasman.2012.01.026.

[25] P.W. Preisler, L. Berger, Oxidation-Reduction Potentials of Thiol-Dithio Systems: Thiourea-Formamidine Disulfide, J. Am. Chem. Soc. 69 (1947) 322–325. doi:10.1021/ja01194a048.

[26] D.R. Lide, ed., CRC Handbook of Chemistry and Physics, 84th ed., CRC Press, Boca Raton, USA, 2003.

[27] M.E. Poisot-Díaz, I. González, G.T. Lapidus, Electrodeposition of a Silver-Gold Alloy (DORÉ) from Thiourea Solutions in the Presence of Other Metallic Ion Impurities, Hydrometallurgy. 93 (2008) 23–29. doi:10.1016/J.HYDROMET.2008.02.015.

[28] M. Ameyama, E. Shinagawa, O. Adachi, D-fructose dehydrogenase of gluconobacter industrius: purification, characterization, and application to enzymatic microdetermination of D-Fructose, J. Bacteriol. 145 (1981) 814–823.

[29] K. Matsumoto, O. Hamada, H. Ukeda, Y. Osajima, Amperometric flow injection determination of fructose with an immobilized fructose 5-dehydrogenase reactor, Anal. Chem. 58 (1986) 2732–2734. doi:10.1021/ac00126a033.

[30] K. Matsumoto, H. Kamikado, H. Matsubara, Y. Osajima, Simultaneous Determination of Glucose, Fructose, and Sucrose in Mixtures by Amperometric Flow Injection Analysis with Immobilized Enzyme Reactors, Anal. Chem. 60 (1988) 147–151. doi:10.1021/ac00153a010.

[31] T. Ikeda, F. Fushimi, K. Miki, M. Senda, Amperometric biosensors based on quinoproteine-, flavoproteine-dehydrogenases; Methods of steady-state current measurements and voltammetric measurements at higher sensitivity, Bunseki Kagaku. 38 (1989) 583–588. doi:10.2116/bunsekikagaku.38.11_583.

[32] X. Xie, S.S. Kuan, G.G. Guilbault, A Simplified Fructose Biosensor, Biosens. Bioelectron. 6 (1991) 49–54. doi:10.1016/0956-5663(91)85008-K.

[33] M. Tominaga, C. Shirakihara, I. Taniguchi, Direct heterogeneous electron transfer reactions and molecular orientation of fructose dehydrogenase adsorbed onto pyrolytic graphite electrodes, J. Electroanal. Chem. 610 (2007) 1–8. doi:10.1016/j.jelechem.2007.06.014.

[34] Y. Sugimoto, Y. Kitazumi, O. Shirai, M. Yamamoto, K. Kano, Role of 2-mercaptoethanol in direct electron transfer-type bioelectrocatalysis of fructose dehydrogenase at Au electrodes, Electrochim. Acta. 170 (2015) 242–247. doi:10.1016/j.electacta.2015.04.164.

[35] K. Murata, M. Suzuki, K. Kajiya, N. Nakamura, H. Ohno, High performance bioanode based on direct electron transfer of fructose dehydrogenase at gold nanoparticle-modified electrodes, Electrochem. Commun. 11 (2009) 668–671. doi:10.1016/j.elecom.2009.01.011.

[36] C. Léger, A.K. Jones, S.P.J. Albracht, F.A. Armstrong, Effect of a Dispersion of Interfacial Electron Transfer Rates on Steady State Catalytic Electron Transport in [NiFe]-hydrogenase and Other Enzymes, J. Phys. Chem. B. 106 (2002) 13058–13063. doi:10.1021/JP0265687.

[37] C. Léger, P. Bertrand, Direct Electrochemistry of Redox Enzymes as a Tool for Mechanistic Studies, Chem. Rev. 108 (2008) 2379–2438. doi:10.1021/cr0680742.

[38] Y. Okawa, N. Yokoyama, Y. Sakai, F. Shiba, Direct electron transfer biosensor for hydrogen peroxide carrying nanocomplex composed of horseradish peroxidase and Au-nanoparticle – Characterization and application to bienzyme systems, Anal. Chem. Res. 5 (2015) 1–8. doi:10.1016/j.ancr.2015.05.001.

[39] M. Tominaga, S. Nomura, I. Taniguchi, d-Fructose detection based on the direct heterogeneous electron transfer reaction of fructose dehydrogenase adsorbed onto multi-walled carbon nanotubes synthesized on platinum electrode, Biosens. Bioelectron. 24 (2009) 1184–1188. doi:10.1016/j.bios.2008.07.002.

[40] Y. Kamitaka, S. Tsujimura, K. Kano, High Current Density Bioelectrolysis of D-Fructose at Fructose Dehydrogenase-adsorbed and Ketjen Black-modified Electrodes without a Mediator, Chem. Lett. 36 (2007) 218–219. doi:10.1246/cl.2007.218.

[41] X. Wu, F. Zhao, J.R. Varcoe, A.E. Thumser, C. Avignone-Rossa, R.C.T. Slade, A one-compartment fructose/air biological fuel cell based on direct electron transfer, Biosens.

Bioelectron. 25 (2009) 326–331. doi:10.1016/j.bios.2009.07.011.

[42] M.J. Swann, D. Bloor, T. Haruyama, M. Aizawa, The role of polypyrrole as charge transfer mediator and immobilization matrix for D-fructose dehydrogenase in a fructose sensor, Biosens. Bioelectron. 12 (1997) 1169–1182. doi:10.1016/S0956-5663(97)00087-0.

[43] T. Kuwahara, M. Kameda, K. Isozaki, K. Toriyama, M. Kondo, M. Shimomura, Bioelectrocatalytic fructose oxidation with fructose dehydrogenase-bearing conducting polymer films for biofuel cell application, React. Funct. Polym. 116 (2017) 87–91. doi:10.1016/j.reactfunctpolym.2017.04.011.

[44] K. Murata, M. Suzuki, N. Nakamura, H. Ohno, Direct evidence of electron flow via the heme c group for the direct electron transfer reaction of fructose dehydrogenase using a silver nanoparticle-modified electrode, Electrochem. Commun. 11 (2009) 1623–1626. doi:10.1016/j.elecom.2009.06.012.

Figure Captions

Fig. 1 Transmission electron micrograph of developed silver (pAgNF) (a) and gold-deposited pAgNF (hAuAgNS) (b). Scanning electron micrograph of gold-deposited pAgNF (hAuAgNS) (c). A typical TEM-EDX spectrum (d, left) and the corresponding TEM image (d, right) of hAuAgNS (the red circle in the right panel indicates the excitation region for the EDX analysis).

Fig. 2 Cyclic voltammograms for FDH-hAuAgNS electrode in the pH 6.5 phosphate buffer in the absence (left, blue lines) and presence (right, red lines) of 0.2 mol dm^{-3} fructose at successively expanding scanning potential ranges under stirring. Scan rate, 50 mV s^{-1}; start potential, –0.2 V. Cross at each curve indicates the corresponding potential-current origin.

Fig. 3 Time course of the response of the FDH-hAuAgNS electrode to the successive additions of fructose at 0.20 V vs Ag/AgCl. Parameters show the fructose concentration after each addition. The solution was continuously stirred, but the stirring stopped during the periods indicated by the red arrows.

Fig. 4 Calibration graphs for modified electrodes for fructose. ●, hAuAgNS; △, AuNP; □, pAgNF. Working potential, +0.2 V vs Ag/AgCl.

Fig. 5 Calibration graph for FDH/hAuAgNS electrodes. Base electrode, carbon paper (■, ▲), ITO (○). Loaded amount, 5×10^{-7} mol-Ag cm^{-2} (○, ▲), 2×10^{-6} mol-Ag cm^{-2} (■).

Table 1. Standard potentials E^o for half reactions relevant to the hAuAgNS formation.

Reaction	E^o / V vs. SHE	Ref.
formamidine^{2+} + 2e = 2 thiourea	+0.420	[25]
Au^{3+} + 2e = Au^{+}	+1.401	[26]
Au(thiourea)$^{2+}$ + e = Au^0 + 2 thiourea	+0.380	[23]
Ag_2(thiourea)$_3^{2+}$ + 2e = 2 Ag_0 + 3 thiourea	+0.04	[27]*

*The potential was calculated from thermodynamic data given in the literature.